

# Mechanistic modeling of micro-drilling cutting forces

Ravi Shankar Anand<sup>1</sup> · Karali Patra<sup>2</sup> · Markus Steiner<sup>3</sup> · Dirk Biermann<sup>3</sup>

Received: 28 February 2015 / Accepted: 16 March 2016 / Published online: 23 April 2016  
© Springer-Verlag London 2016

**Abstract** This paper presents a mechanistic model for micro-drilling cutting forces that includes the cutting edge radius and the minimum chip thickness size effects. The proposed model considers three different cutting regions, i.e., ploughing-dominant, transition, and shearing-dominant, based on these size effects. Specific normal force and specific friction force coefficients have been determined through model calibration using micro-drilling experimental results. Model is validated with micro-drilling experimental results of different cutting conditions and of different machining environments. Comparisons of model simulated and experimental results show that ploughing force contributions are significant, especially at low feed rates. The proposed model has also been applied to characterize size effects in micro-drilling.

**Keywords** Micro-drilling · Specific cutting force · Tool edge radius · Minimum chip thickness · Mechanistic model

## Abbreviations

$\eta_c$  Chip flow angle  
 $\varphi$  Chisel edge angle  
 $\eta_c$  Chip flow angle

$\alpha_e$  Effective rake angle  
 $\alpha_p$  Effective rake angle in ploughing  
 $\alpha_s$  Effective rake angle in transition  
 $\delta x$  Elemental radial distance  
 $\delta F_{lat}$  Elemental lateral force  
 $\delta F_x$  Elemental radial force in  $x$  direction  
 $\delta F_y$  Elemental radial force in  $y$  direction  
 $\delta F_\xi$  Elemental radial force in  $\xi$  direction  
 $\delta F_\eta$  Elemental radial force in  $\eta$  direction  
 $\delta F_{thu}$  Elemental thrust force  
 $\delta F_z$  Elemental thrust force in  $z$  direction  
 $\phi$  Half-point angle  
 $h$  Helix angle  
 $i$  Inclination angles  
 $t_s$  Limiting value of chip thickness for shearing  
 $t_{mc}$  Minimum chip thickness  
 $\alpha_c$  Normal rake angle at chisel edge  
 $\alpha_n$  Normal rake angle at major cutting edge  
 $r$  Radial distance of drill  
 $K_{ns}$  Specific normal force shearing  
 $K_f$  Specific friction force  
 $K_{fp}$  Specific friction force in ploughing  
 $K_{fs}$  Specific friction force in shearing  
 $r_e$  Tool edge radius  
 $A_c$  Undeformed chip area  
 $t$  Undeformed chip thickness  
 $2w$  Web thickness

✉ Karali Patra  
kpatra@iitp.ac.in

<sup>1</sup> Department of Mechanical Engineering, Birla Institute of Technology, Patna campus, Patna 800014, India  
<sup>2</sup> Department of Mechanical Engineering, Indian Institute of Technology Patna, Bihta Patna 801103, India  
<sup>3</sup> Institute of Machining Technology, TU Dortmund, Dortmund 44227, Germany

## 1 Introduction

Micro-holes are important micro-features of many industrial components such as electromechanical system (MEMS), printed circuit boards in electronics products, fuel injection nozzles, filters, flow measuring devices, and cooling channels

in turbine blades [1]. In general, laser beam machining, ultrasonic machining, electrochemical machining (ECM), electrodischarge machining (EDM), and micro-drilling are used to produce micro-holes [2]. Among these methods, micro-drilling is now gaining more acceptability because it has high material removal rate compared to many nonconventional micro-machining processes and wide applicability to most of the engineering materials [3].

In mechanical micro-machining which includes micro-milling, micro-turning, and micro-drilling, undeformed chip thickness is comparable to cutting tool edge radius [4]. In such condition, effective rake angle during chip formation becomes highly negative and specific cutting force of the mechanical micro-machining increases [5]. It may also happen that chip formation does not take place when the feed is below a minimum chip thickness where material plastically deforms under the edge of the tool, and the rest elastically recovers [6]. These characteristics are commonly known as size effects in mechanical micro-machining processes [7]. Klocke et al. [8] characterized the various size effects and their significant influences on the micro-drilling of steel with the help of the experimental results and successfully extended the conventional metal cutting formula of Victor Kienzle in modeling of the micro-drilling feed forces. Anand et al. [9] also analyzed the size effect phenomenon in micro-drilling of carbon-reinforced fiber plastic. Specific feed force and specific radial forces were shown to increase nonlinearly with decrease of uncut chip thickness.

It is important to predict cutting forces in micro-machining as the cutting forces are related to tool life, product quality, and productivity. Therefore, several attempts have been reported to predict the cutting forces with consideration of tool edge radius effect in micro-machining using analytical method, finite element method, and mechanistic modeling techniques, with most of the contributions related to micro-milling process [10, 11]. Rao and Shunmugam [12] developed analytical force model for the micro-end milling operation with consideration of the material strengthening as well as the tool edge radius effects. Lai et al. [13] proposed a finite element model for micro-scale milling process considering tool edge radius and explained that specific shear energy increases greatly due to ploughing when the uncut chip thickness is smaller than minimum chip thickness. Jun et al. [14] developed a mechanistic model of micro-end milling forces, with consideration of the effects of ploughing, elastic recovery, effective rake angle, and flank face rubbing. Two different mechanistic models were used for shearing-dominant and ploughing-dominant regimes due to tool edge radius effect [15].

Contrary to many cutting force modeling attempts in micro-milling, very few modeling works have been reported in the area of micro-drilling so far. Hinds and Treanor [16] developed finite element methods to analyze the stresses in micro-drilling of printed circuit boards. However, they did not provide any mathematical modeling for drilling forces. Gong et al. [17]

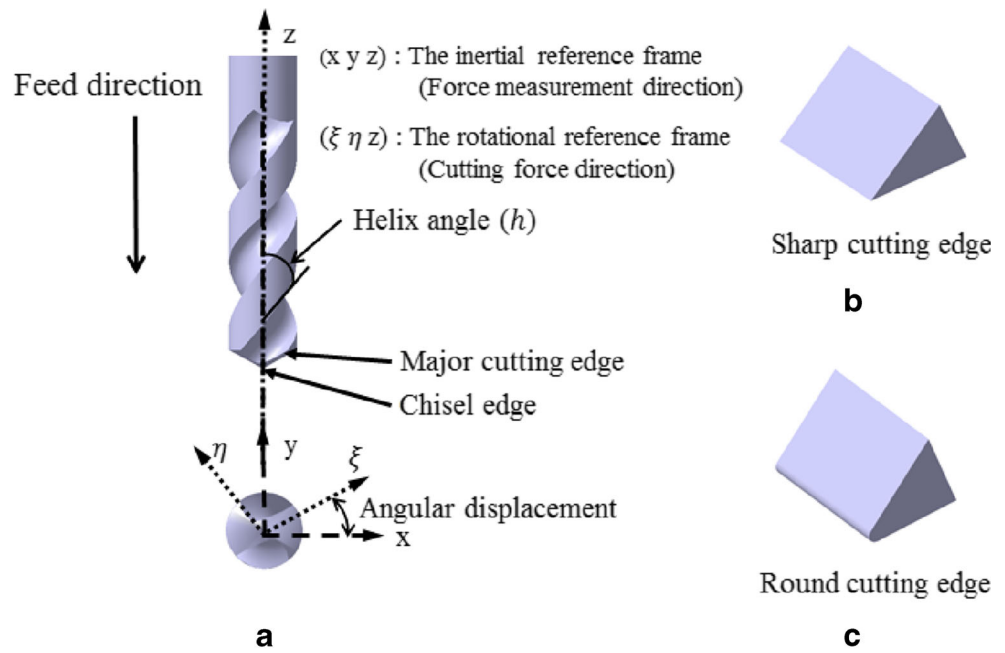
developed a mechanistic model of micro-drilling in which cutting forces were determined in terms of specific normal and friction forces and their coefficients were determined from cutting experiments. Tool run out, installation error, and tool grinding errors were considered for modeling dynamic cutting forces. However, tool edge radius effects were not considered. Sambhav et al. [18] developed a slip line field-based analytical cutting force model of micro-drilling with consideration of tool edge radius effect and minimum chip thickness effects on major cutting edge. Thrust force contribution from chisel edge was not included in their analysis. Chisel edge of micro-drill not only effectively contributes to rigidity and stability of tool during micro-drilling but also contributes with large share of thrust force which affects the tool life of slender micro-drill significantly [8, 19]. Hence, it is essential to model the chisel edge contribution of thrust force also. Zhang et al. [20] extended the slip line field-based analytical model to include the contribution of chisel edge to micro-drilling thrust force. Rahamathullah and Shunmugam [21] developed a mechanistic model to predict micro-drilling thrust and torque, considering material removal in major cutting edges, chisel edge, and indentation zones. However, their proposed mechanistic models did not consider tool edge radius effects as large uncut chip thickness values were used.

This article presents a mechanistic micro-drilling force model with consideration of tool edge radius and minimum chip thickness. Tool edge radius mainly affects the effective rake angle that varies according to undeformed chip thickness. Effect of ploughing is also considered for undeformed chip thickness lower than the minimum chip thickness. Three different cutting regions, viz., ploughing-dominant, transition, and shearing-dominant, have been assumed for both major cutting edge and chisel edge on the basis of uncut chip thickness value. The proposed mechanistic model has been validated from experimental results of micro-drilling of austenitic stainless steel using 0.5-mm-diameter tungsten carbide drills. Comparisons of mechanistic model simulations with and without tool edge radius effects have also been shown with experimental results. The proposed model has also been used to characterize the size effects in the micro-drilling process.

## 2 Model development

Figure 1a shows the pictorial view of a drill bit with feed direction and reference frames used for developing mechanistic model of the drilling process. The inertial frame ( $x, y, z$ ) is a fixed coordinate system and aligned with the dynamometer coordinate system. The rotational reference frame ( $\xi, \eta, z$ ) axis is attached to the drill body in which  $\xi$  axis is in the direction of the major cutting edge, the  $\eta$  axis is perpendicular to the major cutting edge, and the  $z$  axis is along the drill axis as shown in Fig. 1a. The instantaneous position of the rotational frame of reference with respect to the inertial frame has also

**Fig. 1** Pictorial view of drill bit showing **a** feed direction, reference frames **b** sharp edge assumption for conventional drilling and **c** round cutting edge for micro-drilling



been shown in Fig. 1a by angular displacement due to the rotation of the drill bit. Cutting forces in the mechanistic model are generally defined in the rotational frame of reference. For the calibration of the model, cutting forces of rotational reference frame are transformed to the inertial frame where force measurements are performed. Although geometrically drill bits are similar in both conventional and micro-drilling, the chip thickness is comparable to the cutting tool edge radius in case of micro-drilling. Round cutting edge is considered in micro-drilling (Fig. 1c) instead of sharp cutting edge assumption of conventional drilling (Fig. 1b) for the development of mechanistic cutting force model.

The basic cutting mechanism of micro-drilling is described as the combination of oblique cutting on major cutting edge and orthogonal cutting on chisel edge [22]. In mechanistic modeling process, normal force ( $F_n$ ) and friction force ( $F_f$ ) are assumed to be proportional to the undeformed chip area [17] as given in Eqs. (1) and (2):

$$F_n = K_n A_c \tag{1}$$

$$F_f = K_f A_c \tag{2}$$

where  $K_n$  and  $K_f$  are the specific normal and frictional forces and  $A_c$  is the undeformed chip area. The cutting force, thrust force, and lateral force are then related to friction and normal forces through process kinematics and drill geometrical parameters. The basis for development of the new model in this work is the oblique cutting model developed by Gong et al. [17] for conventional drilling where tool edge radius effect was neglected. Major cutting edge forces and chisel edge forces with consideration of tool edge radius and minimum chip thickness effects are described in the following section.

Cutting forces without tool edge radius effects are also described in the following sections.

## 2.1 Forces in major cutting edge

### 2.1.1 Cutting forces without tool edge radius effect

In conventional drilling model, cutting edge is considered as sharp. The cutting action along the major cutting edge can be interpreted as a series of oblique sections as shown in Fig. 2a. The normal rake angle ( $\alpha_n$ ) and inclination angles ( $i$ ) as shown in Fig. 2b vary along radial distance ( $r$ ) and are defined in terms of drill geometry such as helix angle ( $h$ ), half-point angle ( $\phi$ ), and web thickness ( $2w$ ) and shown in Eqs. (3) and (4), respectively [17]:

$$\alpha_n = \tan^{-1} \left( \frac{\sqrt{r^2 - w^2} \tanh h}{r \sin \phi - w \cos \phi \tanh h} \right) - \tan^{-1} \left( \frac{w \cos \phi}{\sqrt{r^2 - w^2}} \right) \tag{3}$$

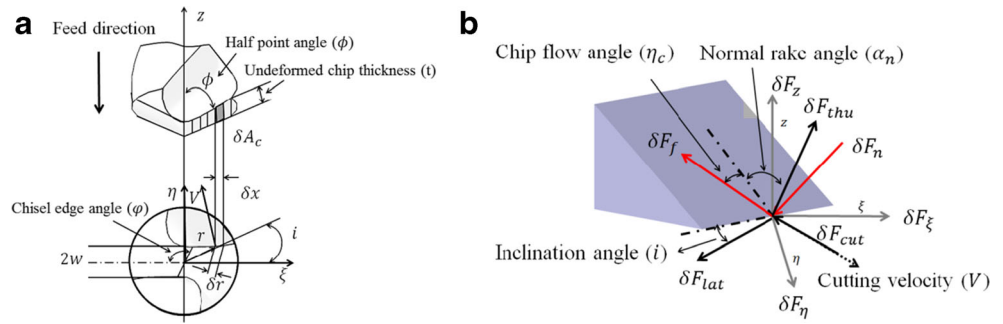
$$i = \sin^{-1} (w \sin \phi / r) \tag{4}$$

The undeformed chip thickness ( $t$ ) can be obtained from feed ( $f$ ) and the point angle of the drill as given in Eq. (5):

$$t = 0.5 f \sin \phi \tag{5}$$

The width of cut in the plane whose normal is coincident with the direction of the cutting velocity ( $V$ ) depends on

**Fig. 2 a** Drill Geometry and **b** cutting force components in cutting edge [17]



inclination angle, point angle, and elemental radial distance ( $\delta x$ ), and product with undeformed chip thickness gives the elemental chip area ( $\delta A_c$ ) as shown in Eq. (6):

$$\delta A_c = t \delta x \cos i / \sin \phi \tag{6}$$

Major cutting edge forces in conventional drilling process can be shown in Fig. 2b. Major cutting edge is divided into numbers of small elements which can be assumed as straight cutting edges. Therefore, Stabler’s rule [23] can be valid here and the chip flow angle ( $\eta_c$ ) is equal to inclination angle ( $i$ ) of a particular element. The chip flow angle varies along the entire cutting edge with the variation of the inclination angle. The elemental cutting force ( $\delta F_{cut}$ ) acts opposite to the velocity direction. The elemental oblique cutting thrust force ( $\delta F_{thu}$ ) is normal to the plane that contains the velocity vector and the cutting edge. The elemental lateral force ( $\delta F_{lat}$ ) is orthogonal to the cutting force and thrust force [17].

The magnitude of the elemental lateral force, cutting force, and thrust force can be computed from the elemental normal force and friction force from Eqs. (7), (8), and (9), respectively:

$$\delta F_{lat} = \delta F_f (\cos \eta_c \sin i \sin \alpha_n - \sin \eta_c \cos i) + \delta F_n \cos \alpha_n \sin i \tag{7}$$

$$\delta F_{cut} = \delta F_f (\cos \eta_c \cos i \sin \alpha_n + \sin \eta_c \sin i) + \delta F_n \cos \alpha_n \cos i \tag{8}$$

$$\delta F_{thu} = \delta F_f \cos \eta_c \cos \alpha_n - \delta F_n \sin \alpha_n \tag{9}$$

where  $\delta F_f = K_f \delta A_c$  and  $\delta F_n = K_n \delta A_c$ , and  $K_n$  and  $K_f$  are the specific normal and frictional force, respectively.

2.1.2 Cutting force with tool edge radius and minimum chip thickness effects

Jun et al. [14] considered three different cutting regions, namely, ploughing-dominant, transition, and shearing-dominant with consideration of tool edge radius effect and minimum chip thickness effects for mechanistic modeling of

micro-milling. However, the elemental cutting force components were computed assuming the cutting process as orthogonal cutting. Similarly, Klocke et al. [8] showed experimentally that above three different cutting regions existed in micro-drilling also. Three different cutting regions depending on the undeformed chip thickness as shown in Fig. 3 are also assumed in this model. However, elemental cutting forces are computed considering oblique cutting in the major cutting edge of the micro-drill. Ploughing effect dominates without chip formation below the minimum chip thickness  $t_{mc}$ . When chip thickness is above minimum chip thickness, chip formation will take place with ploughing effects. The effective rake angle becomes negative and varies according to the undeformed chip thickness. This transition region exists till undeformed chip thickness equals to  $t_s$ , where  $t_s = r_e (1 + \sin \alpha_n)$ . Above the transition region, i.e., when undeformed chip thickness is above  $t_s$ , the cutting process is shearing-dominant and effective rake angle becomes equal to the normal rake angle ( $\alpha_n$ ).

Figure 4 shows the variation of normal rake angle with the radial distance of the major cutting edge for a 0.5-mm-diameter drill with geometrical parameters given in Table 1. It also shows how the effective rake angle varies with undeformed chip thickness in the major cutting edge. Vertical lines “ABC” and “EF” illustrate how the values of the effective rake angle can be obtained for different values of undeformed chip thickness in two regions, i.e., one with positive normal rake angle ( $t_s > r_e$ ) and the another with negative normal rake angle ( $t_s < r_e$ ).

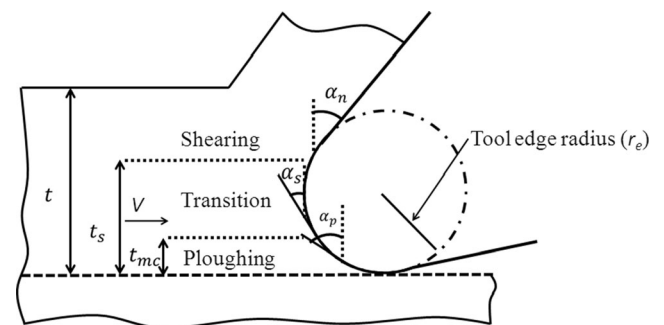


**Fig. 3** Tool edge radius effect on major cutting edge

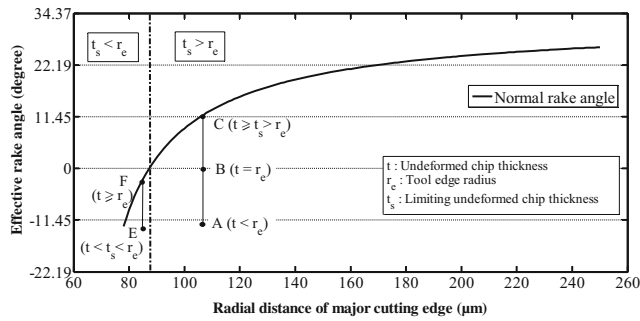


**Fig. 4** Determination of effective rake angle in the major cutting edge

The cutting forces in ploughing, transition, and shearing regions are given as follows.

**Ploughing-dominant region ( $0 < t < t_{mc}$ )** In this region, the effective rake angle ( $\alpha_e$ ) is constant along the major cutting edge and it varies according to undeformed chip thickness. The effective rake angle ( $\alpha_p$ ) in the ploughing region can be obtained by Eq. (10) [4]. Ploughing force components in lateral, cutting, and thrust directions can be determined by Eqs. (11), (12), and (13), respectively:

$$\alpha_p = \alpha_e = \sin^{-1} \left( \frac{t - r_e}{r_e} \right) \tag{10}$$

$$\delta F_{lat} = \delta F_{fp} (\cos \eta_c \sin i \sin \alpha_p - \sin \eta_c \cos i) + \delta F_{np} \cos \alpha_p \sin i \tag{11}$$

$$\delta F_{cut} = \delta F_{fp} (\cos \eta_c \cos i \sin \alpha_p + \sin \eta_c \sin i) + \delta F_{np} \cos \alpha_p \cos i \tag{12}$$

$$\delta F_{thu} = \delta F_{fp} \cos \eta_c \cos \alpha_p - \delta F_{np} \sin \alpha_p \tag{13}$$

where

$\delta F_{fp} = K_{fp} \delta A_{cp}$  and  $\delta F_{np} = K_{np} \delta A_{cp}$ .  $K_{np}$  and  $K_{fp}$  are the specific normal and frictional force in ploughing, respectively.  $\delta A_{cp}$  is the elemental undeformed chip area in plough-dominant region.

**Table 1** Geometrical parameters of drill bits

Drill diameter ( $d$ )	0.5 mm
Point angle ( $\phi$ )	128°
Helix angle ( $h$ )	30°
Clearance angle ( $\lambda$ )	10°
Web thickness ( $2w$ )	0.134 mm
Chisel edge angle ( $\varphi$ )	128°
Tool edge radius ( $r_e$ )	2.5 µm

**Transition region ( $t_{mc} < t < t_s$ )** The effective rake angle depends on uncut chip thickness also in the transition region, and it is given by Eq. (14). The effective rake angle ( $\alpha_s$ ) is highly negative and remains constant along the major cutting edge. Cutting force components in lateral, cutting, and thrust directions can be determined by Eqs. (15), (16), and (17), respectively:

$$\alpha_s = \alpha_e = \sin^{-1} \left( \frac{t - r_e}{r_e} \right) \tag{14}$$

$$\delta F_{lat} = \delta F_{fs} (\cos \eta_c \sin i \sin \alpha_s - \sin \eta_c \cos i) + \delta F_{ns} \cos \alpha_s \sin i \tag{15}$$

$$\delta F_{cut} = \delta F_{fs} (\cos \eta_c \cos i \sin \alpha_s + \sin \eta_c \sin i) + \delta F_{ns} \cos \alpha_s \cos i \tag{16}$$

$$\delta F_{thu} = \delta F_{fs} \cos \eta_c \cos \alpha_s - \delta F_{ns} \sin \alpha_s \tag{17}$$

where

$\delta F_{fs} = K_{fs} \delta A_{cs}$  and  $\delta F_{ns} = K_{ns} \delta A_{cs}$ .  $K_{ns}$  and  $K_{fs}$  are the specific normal and frictional force in shearing, respectively.  $\delta A_{cs}$  is the elemental undeformed chip area in shearing.

**Shearing-dominant region ( $t \geq t_s$ )** When uncut chip thickness is above  $t_s$ , the effective rake angle is equal to the normal rake angle of major cutting edge as shown in Eq. (18). Cutting force components in lateral, cutting, and thrust directions in shearing-dominant region can be determined by Eqs. (19), (20), and (21), respectively:

$$\alpha_e = \alpha_n \tag{18}$$

$$\delta F_{lat} = \delta F_{fs} (\cos \eta_c \sin i \sin \alpha_n - \sin \eta_c \cos i) + \delta F_{ns} \cos \alpha_n \sin i \tag{19}$$

$$\delta F_{cut} = \delta F_{fs} (\cos \eta_c \cos i \sin \alpha_n + \sin \eta_c \sin i) + \delta F_{ns} \cos \alpha_n \cos i \tag{20}$$

$$\delta F_{thu} = \delta F_{fs} \cos \eta_c \cos \alpha_n - \delta F_{ns} \sin \alpha_n \tag{21}$$

The elemental drilling cutting forces ( $dF_{thu}$ ,  $dF_{cut}$  and  $dF_{lat}$ ) obtained from above equations are then transformed into elemental radial forces ( $\delta F_\xi$  and  $\delta F_\eta$ ) and thrust force ( $\delta F_z$ ) in rotational coordinate frame as shown in Eqs. (22), (23), and (24), respectively [17]:

$$\delta F_\xi = \delta F_{thu} \frac{-\cos v \sin \phi}{\cos i} + \delta F_{cut} \sin v - \delta F_{lat} \frac{\cos v \cos v \sin \phi}{\cos i} \tag{22}$$

$$\delta F_{\eta} = \delta F_{thu} \frac{-\sin v \sin \phi}{\cos i} - \delta F_{cut} \cos v - \delta F_{lat} \frac{\cos v \sin v \sin \phi}{\cos i} \tag{23}$$

$$\delta F_z = \delta F_{thu} \frac{\cos v \sin \phi}{\cos i} - \delta F_{lat} \frac{\cos \phi}{\cos i} \tag{24}$$

where  $v = \sin^{-1}(w/r)$  is the angle between chisel edge length and elemental radial distance with respect to cutting velocity direction.

Total thrust and radial forces for major cutting edges can be obtained by summing the respective forces at all elements for both major cutting edges.

### 2.2 Forces in chisel edge

#### 2.2.1 Chisel edge cutting force without tool edge radius effect

The cutting process of the chisel edge (secondary cutting edge) can be viewed as an orthogonal cutting process [17], which means that the inclination angle and the lateral force at the chisel edge are equal to zero. The orthogonal cutting action along chisel edge with constant normal rake angle ( $\alpha_c$ ) that can be computed from the point angle of the drill and the chisel edge angle ( $\varphi$ ) is shown in Eq. (25) [17]:

$$\alpha_c = -\tan^{-1}(\tan \phi \cos(\pi - \varphi)) \tag{25}$$

The undeformed chip thickness in chisel edge is determined by the following Eq. (26), where  $\alpha_\gamma$  is the angle between cutting speed and feed speed [24]:

$$t = 0.5f \cos \alpha_\gamma \tag{26}$$

The thrust force and cutting force of an element on the secondary cutting edge can be given by the following Eqs. (27) and (28), respectively. Cutting velocity direction, cutting force directions, and angles in chisel edge are shown in Fig. 5.

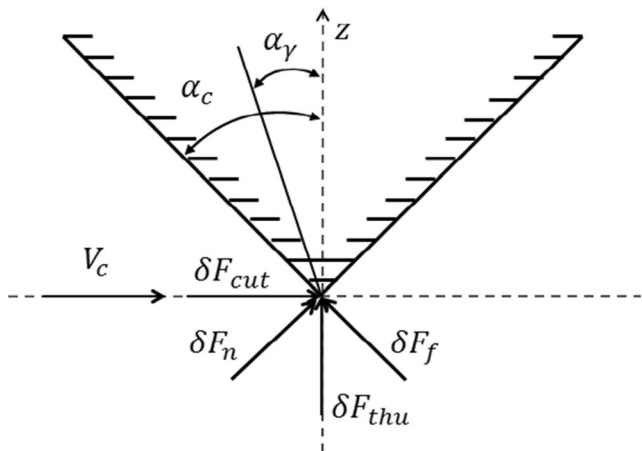


Fig. 5 Cutting forces of chisel edge

$$\delta F_{th} = \delta F_f \cos \alpha_c - \delta F_n \sin \alpha_c \tag{27}$$

$$\delta F_{cut} = \delta F_f \sin \alpha_c + \delta F_n \cos \alpha_c \tag{28}$$

where

$$\delta F_f = K_f \delta A_c \text{ and } \delta F_n = K_n \delta A_c.$$

$K_n$  and  $K_f$  are the normal and frictional specific cutting forces, respectively.

$\delta A_c$  is the elemental undeformed chip area of chisel edge.

#### 2.2.2 Cutting force with tool edge radius and minimum chip thickness effect

Due to the limitations of the conventional grinding processes, most of the cutting edges have finite edge radius in the range of few micro-meters [3]. In micro-machining, the chip thickness is comparable to the cutting edge radius and the cutting edge cannot be considered as sharp edge. The same argument is also applicable for chisel edge, and it is considered as round edge instead of sharp edge assumed in conventional drilling [20]. Similar to major cutting edge, three different regions, namely, ploughing region, transition region, and shearing-dominant region, are considered in chisel edge cutting force model in micro-drilling. However, elemental cutting force components in chisel edge are computed assuming the cutting process as orthogonal cutting.

The elemental cutting forces in ploughing, transition, and shearing regions of the chisel edge are given as follows.

**Ploughing-dominant region ( $0 < t < t_{mc}$ )** Below minimum chip thickness, ploughing action takes place without chip removal. Effective rake angle in ploughing region depends on the undeformed chip thickness and is given by Eq. (10). Ploughing force components in thrust and cutting directions can be determined by Eqs. (29) and (30), respectively:

$$\delta F_{th} = \delta F_{fp} \cos \alpha_p - \delta F_{np} \sin \alpha_p \tag{29}$$

$$\delta F_{cut} = \delta F_{fp} \sin \alpha_p + \delta F_{np} \cos \alpha_p \tag{30}$$

where

$$\delta F_{fp} = K_{fp} \delta A_{cp} \text{ and } \delta F_{np} = K_{np} \delta A_{cp}.$$

$K_{np}$  and  $K_{fp}$  are the normal and frictional specific cutting forces, respectively.

$\delta A_{cp}$  is the elemental undeformed chip area in ploughing-dominant region of chisel edge.

**Transition region ( $t_{mc} < t < t_s$ )** When undeformed chip thickness is above minimum chip thickness, shearing will take place with ploughing effect. Effective rake angle will vary with the undeformed chip thickness till uncut chip thickness reaches the limiting value  $t_s$ . The effective rake angle in transition is given by Eq. (14). Cutting force components in thrust and cutting directions in this region can be determined by Eqs. (31) and (32), respectively:

$$\delta F_{th} = \delta F_{fs} \cos \alpha_s - \delta F_{ns} \sin \alpha_s \tag{31}$$

$$\delta F_{cut} = \delta F_{fs} \sin \alpha_s + \delta F_{ns} \cos \alpha_s \tag{32}$$

where

$$\delta F_{fs} = K_{fs} \delta A_{cs} \text{ and } \delta F_{ns} = K_{ns} \delta A_{cs}.$$

$K_{ns}$  and  $K_{fs}$  are the normal and frictional specific cutting forces in shearing, respectively.

$\delta A_{cs}$  is the elemental undeformed chip area in shearing in chisel edge.

**Shearing-dominant region ( $t \geq t_s$ )** The third region is the shearing-dominant where chip formation takes place with effective rake angle equal to the normal rake angle of the chisel edge (Eq. (33)) as shown in Fig. 6. Cutting force components in thrust and cutting velocity directions can be determined by Eqs. (34) and (35), respectively:

$$\alpha_e = \alpha_c \tag{33}$$

$$\delta F_{th} = \delta F_{fs} \cos \alpha_c - \delta F_{ns} \sin \alpha_c \tag{34}$$

$$\delta F_{cut} = \delta F_{fs} \sin \alpha_c + \delta F_{ns} \cos \alpha_c \tag{35}$$

The elemental drilling cutting forces ( $dF_{thu}$  and  $dF_{cut}$ ) obtained from above equations are then transformed into

elemental radial forces ( $\delta F_\xi$  and  $\delta F_\eta$ ) and thrust force ( $\delta F_z$ ) in rotational coordinate frame and shown by Eqs. (36), (37), and (38), respectively [17]:

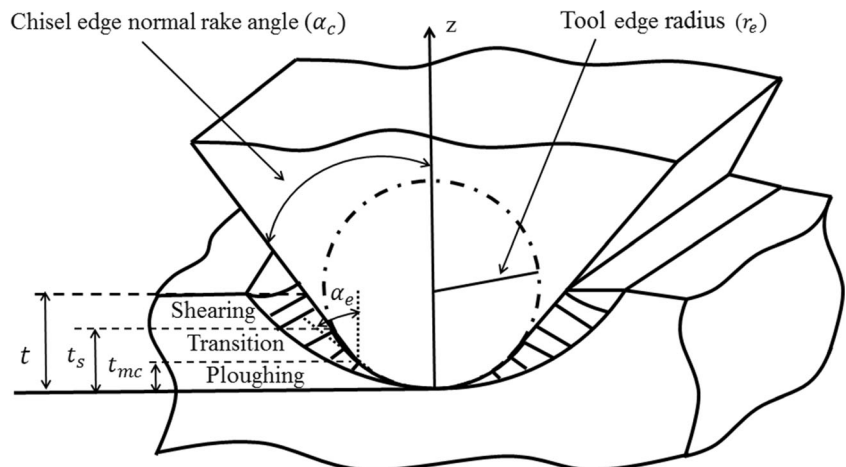
$$\delta F_\xi = \delta F_{cut} \sin \varphi \tag{36}$$

$$\delta F_\eta = -\delta F_{cut} \cos \varphi \tag{37}$$

$$\delta F_z = \delta F_{thu} \tag{38}$$

Many earlier research works on modeling of conventional drilling [17, 22] and modeling of micro-drilling [20, 21] considered that cutting phenomenon acted on a part of the chisel edge and indentation phenomenon occurs in the other part very close to the axis of the drill. However, contribution of indentation zone on cutting force was assumed to be negligible in a mechanistic modeling for high-speed drilling [24]. It has also been observed in this work that indentation radius obtained from the conventional drilling formulation [25] is very small as very small feed value (less than 10  $\mu\text{m}/\text{rev}$ ) has been considered in this work. The maximum indentation radius can be obtained as 5.12  $\mu\text{m}$  at the larger feed value of 10  $\mu\text{m}$  using the conventional formulation as mentioned in [25]. The indentation radius is comparatively very less with respect to total chisels edge length which is about 168  $\mu\text{m}$  in 500- $\mu\text{m}$ -diameter drill. The chisel edge is also assumed as round edge which may take care of the indentation radius effect in micro-drilling process. The thrust force contribution of the indentation zone using conventional approach can be shown to be very small compared to the thrust force of the chisel edge. Hence, indentation zone phenomenon has not considered in this work.

**Fig. 6** Tool edge radius effect on chisel edge



### 2.3 Total thrust force and specific thrust force

Total thrust force of micro-drilling is obtained by summation of all elemental thrust force of major cutting edge and chisel edge from Eq. (39):

$$Fz_{Total} = 2 \times \left( \sum_{chisel} \delta F_z + \sum_{major} \delta F_z \right) \quad (39)$$

Specific thrust force in drilling can be given by dividing total thrust force by total chip area of major and chisel edges. This can be obtained from the following Eq. (40):

$$Th_{spc} = \frac{Fz_{Total}}{\sum \delta A_c} \quad (40)$$

### 3 Experimental setup and model calibration

In order to calibrate the thrust force model, micro-drilling experiments have been performed on austenitic stainless steel (X5CrNi18-10) using 0.5-mm-diameter solid carbide drills. The experimental setup is shown in Fig. 7. The experiments have been conducted in a vertical CNC micro-machining center (Model no: DT110, Mikrottools Pte. Ltd.) in which the linear stage positional accuracy is  $\pm 1 \mu\text{m}$  per 100 mm and travel ranges are 200, 100, and 100 mm in three mutually perpendicular directions, namely, X, Y, and Z, respectively. The machine unit has high-speed spindle speed of up to 60,000 rpm. A piezo electric dynamometer, Kistler Mini Dyn 9256C2, with minimum resolution of 0.002 N is used to measure cutting force components in micro-drilling. A Kistler multi-channel charge amplifier type 5070A converts the charge signals produced by the dynamometer to voltage

**Fig. 7** Experimental setup for micro-drilling of austenitic stainless steel

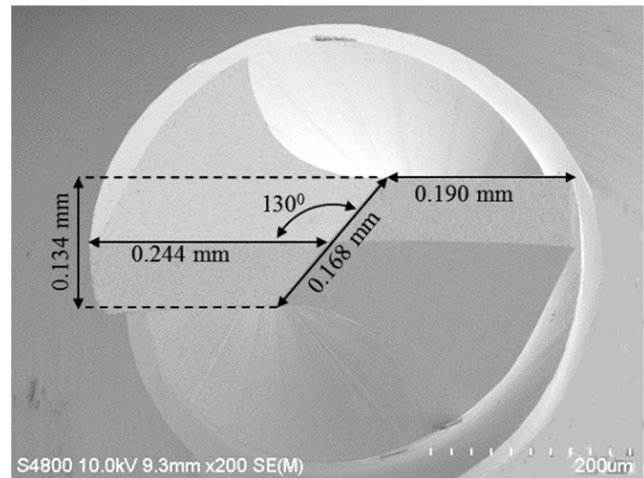
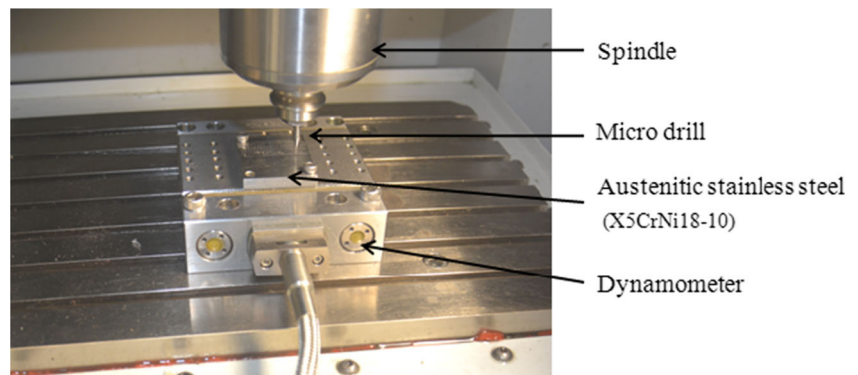


**Fig. 8** End view of 0.5-mm-diameter solid carbide drills

signals and sends to the data acquisition system. Cutting forces data are acquired at a sampling rate of 7142 Hz.

The workpiece material, austenitic stainless steel (X5CrNi18-10), is assumed as a homogeneous material in this work. Standard two fluted solid carbide uncoated drills (0.5-mm diameter) manufactured by Seco Tools GmbH are used in all the drilling experiments. A SEM image of a drill bit is shown in Fig. 8. The major cutting edge length and chisel edge lengths are also shown in this figure. The values of the geometrical parameters of the micro-drill bit are shown in Table 1.

Thrust force is calculated at low to high feed range (0.5, 1, 1.5, 2, 4, and 6  $\mu\text{m}/\text{rev}$ ) with three different maximum cutting speeds as 15.7 m/min (10,000 rpm), 27.5 m/min (17,500 rpm), and 39.2 m/min (25,000 rpm). Since the shearing effect is dominant at high feed and ploughing effect is dominant at low feed, high feed experimental thrust force data are used for finding shearing-specific cutting coefficients and low feed experimental thrust force data are used to determine ploughing coefficients. The experimental results are shown in Table 2.

For calibration of the coefficients of specific normal and frictional forces for ploughing and shearing regions, the error

**Table 2** Experimental thrust force

Sl.	Cutting speed (rpm)	Feed ( $\mu\text{m}/\text{rev}$ )	Undeformed chip thickness ( $\mu\text{m}/\text{rev}$ )	Mean thrust force (N)
1	15.71	0.5	0.224	11.11
2	15.71	1.0	0.449	13.88
3	15.71	1.5	0.673	16.89
4	15.71	2.0	0.898	17.17
5	15.71	4.0	1.796	18.20
6	15.71	6.0	2.694	20.44
7	27.50	0.5	0.224	16.06
8	27.50	1.0	0.449	16.16
9	27.50	1.5	0.673	16.92
10	27.50	2.0	0.898	16.67
11	27.50	4.0	1.796	22.36
12	27.50	6.0	2.694	26.27
13	39.28	0.5	0.224	18.28
14	39.28	1.0	0.449	16.84
15	39.28	1.5	0.673	18.27
16	39.28	2.0	0.898	19.51
17	39.28	4.0	1.796	26.92
18	39.28	6.0	2.694	35.15

between the experimental and model force data is minimized via a nonlinear fitting using Matlab surface fitting tool, “sftool” [15]. Regression equations for specific cutting forces in ploughing and shearing with respect to uncut chip thickness and cutting speed are given in Eqs. (41)–(44):

$$K_{np} \left( \text{N}/\mu\text{m}^2 \right) = 0.00062t^{-1.648}v_c^{0.814} \tag{41}$$

$$K_{fp} \left( \text{N}/\mu\text{m}^2 \right) = 0.04394t^{-0.4408}v_c^{0.00044} \tag{42}$$

$$K_{ns} \left( \text{N}/\mu\text{m}^2 \right) = 0.01953t^{-1.53}v_c^{0.091} \tag{43}$$

$$K_{fs} \left( \text{N}/\mu\text{m}^2 \right) = 0.00855t^{-0.2022}v_c^{0.336} \tag{44}$$

The mean thrust values at a cutting speed of 15.7 m/min and at different feed rates are shown in Fig. 9. It can be observed that the proposed model can appropriately predict the thrust force in the ploughing, transition, and shearing regions. Although cutting force model without tool edge radius and minimum chip thickness can predict

**Fig. 9** Comparison of experimental mean thrust with predicted with and without tool edge radius effect

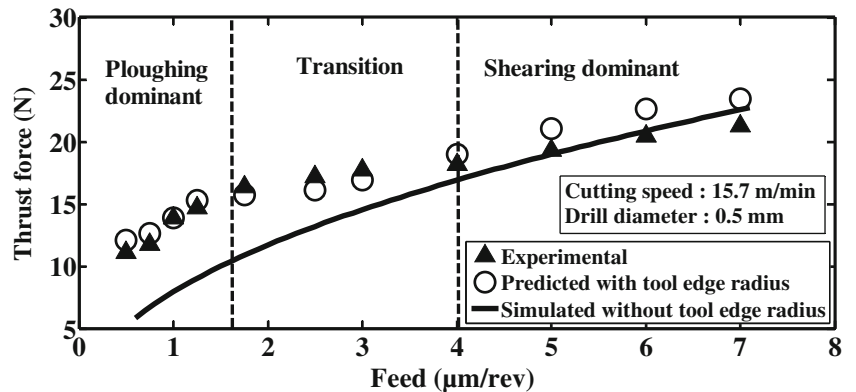


**Table 3** Comparison thrust force prediction performances of model with tool edge radius effect and model without tool edge radius effect for low feed (in ploughing region)

Sl no.	Speed (m/min)	Feed ( $\mu\text{m}/\text{rev}$ )	Exp. thrust force (N)	Pre. thrust force (N)		% deviation	
				With tool edge	Without tool edge	With tool edge	Without tool edge
1	15.71	0.5	11.11	12.07	5.85	8.64	47.34
2	15.71	0.75	11.77	12.63	7.23	7.74	38.57
3	15.71	1	13.88	13.83	8.40	0.45	39.48
4	15.71	1.25	14.7	15.31	9.43	5.49	35.82
5	15.71	1.75	16.39	15.72	11.22	6.03	31.54
Average absolute deviation (%)						5.67	38.55

well the thrust force in shear-dominant region, it is unable to predict the forces in ploughing and transition regions. Ploughing region is considered up to the minimum chip thickness value which is assumed to be approximately 0.3 times of the tool edge radius [14, 26, 27]. In this work, minimum chip thickness value was calculated to be  $0.75 \mu\text{m}$  (for tool edge radius of  $2.5 \mu\text{m}$ ), i.e., feed value of approximately  $1.75 \mu\text{m}/\text{rev}$ . The transition region exists where force still increases nonlinearly with uncut chip thickness close to the minimum chip thickness and up to as high as two times the minimum chip thickness [14]. The ploughing-dominant, transition, and shear-dominant regions can be clearly observed from the experimental results as shown in Fig. 9. In the shearing-dominant region, i.e., for feed larger than approximately  $4 \mu\text{m}/\text{rev}$ , thrust force has a linear trend. In the ploughing-dominant region, i.e., for feed less than approximately  $1.75 \mu\text{m}/\text{rev}$  corresponding to the minimum chip thickness value of  $0.75 \mu\text{m}$ , thrust force has also a linear trend like that of shear-dominant region but it has higher slope. However, in the transition region which connects the ploughing and shearing regions, thrust force does not follow any of the linear trends observed in other two regions as there are combined effects of ploughing and shearing. With increase of feed value, shearing effect dominates and ploughing effect diminishes.

The deviations of predicted thrust forces (with and without tool edge radius effect) with respect to experimental thrust forces at low feed as well as high feed are given in Table 3 and Table 4, respectively. It can be observed that the percentage average absolute deviation of the predicted thrust force without considering tool edge radius model is higher (38.55 %) than that with tool edge radius effect (5.67 %) at low feed as shown in Table 3. The percentage average absolute deviation of the predicted thrust force of the conventional model (without considering tool edge radius) only differs slightly from that of the model with tool edge radius at high feed as shown in Table 4. However, the conventional model, i.e., cutting force model without tool edge radius effect, predicts the values of thrust force closer to the experimental thrust force in shear region in which undeformed chip thickness is large enough compared to the cutting tool edge radius. Therefore, tool edge radius effect is negligible and cutting edge may be assumed as sharp cutting edge. Under this condition, material is only removed by shearing process and ploughing effect is negligible. On the other hand, thrust force model with tool edge radius effect considers the contribution of ploughing effect in cutting process which is mainly applicable for the low feed and transition region. However, consideration of tool edge radius in shear region overestimates the cutting coefficients. Thus,

**Table 4** Comparison thrust force prediction performances of model with tool edge radius effect and model without tool edge radius effect for high feed (transition and shearing regions)

Sl no.	Speed (m/min)	Feed ( $\mu\text{m}/\text{rev}$ )	Exp. thrust force (N)	Pre. thrust force (N)		% deviation	
				With tool edge	Without tool edge	With tool edge	Without tool edge
1	15.71	2.5	17.21	16.13	13.48	9.72	21.67
2	15.71	3	17.72	16.93	14.79	7.11	16.53
3	15.71	4	18.2	18.98	17.13	7.02	5.87
4	15.71	5	19.33	19.54	19.18	1.89	0.73
5	15.71	6	20.44	21.35	21.03	8.19	2.92
6	15.71	7	21.29	22.62	22.73	11.97	6.76
Average absolute deviation (%)						7.65	9.08

predicted thrust force by the proposed model is more with respect to experimental thrust force in the shear region.

## 4 Model validation

### 4.1 Prediction of thrust force

The calibrated mechanistic model has been applied to predict thrust force at new cutting conditions and validated with experimental results. The performance of the proposed model which considered tool edge radius effects has also been compared to that of the conventional mechanistic model without tool edge radius [17]. Figure 10a–c shows the comparison of the proposed model and the conventional mechanistic model with experimental thrust forces at different feed values (1.5, 2.5, and 4  $\mu\text{m}/\text{rev}$ ) at a new cutting speed of 23.5 m/min. The first feed value (1.5  $\mu\text{m}/\text{rev}$ ) is taken from ploughing-dominant feed. The second is taken from transition region feed (2.5  $\mu\text{m}/\text{rev}$ ) where ploughing and shearing together affect the cutting process, and the third feed (2.5  $\mu\text{m}/\text{rev}$ ) is taken from shearing-dominant feed. It can be observed that predicted thrust force by the proposed model is close to the experimental thrust force, whereas conventional mechanistic model predicts very less thrust force for feed values in the ploughing-dominant region as shown in Fig. 10a. However, the difference of predicted thrust force by the conventional model and the proposed model decreases for the feed selected from the transition region where shearing takes place along with ploughing effect as shown in Fig. 10b. Tool edge radius effect is less at high feed due to shearing effect. Therefore, the thrust force model with and without tool edge radius effect show the same predicted value that is very close to the experimental mean thrust force as shown in Fig. 10c. These results show that conventional mechanistic model with sharp edge tool may be still be applicable for high feed values where shearing is pre-dominant and ploughing effect can be ignored. However, for low feed values where uncut chip thickness is comparable to tool edge radius, sharp edge tool modeling approach is not adequate and the proposed model which considered size effects must be considered.

Experimental results from different experimental setups [28] that had been carried out in KERN micro-machining center (model no. HSPC 2522) have also been used for the validation of the proposed model. The machine unit has high-speed spindle speed of up to 50,000 rpm with a radial runout of approximately 3  $\mu\text{m}$ . Experiments were performed on the same workpiece material, i.e., austenitic stainless steel (X5CrNi18-10) with the same drill type (0.5-mm-diameter standard two fluted) and the same drill material (solid carbide uncoated drills) used in the calibration test in the earlier experimental setup. Instead of dry drilling performed in earlier setup, these experiments used mineral-oil-based coolant for

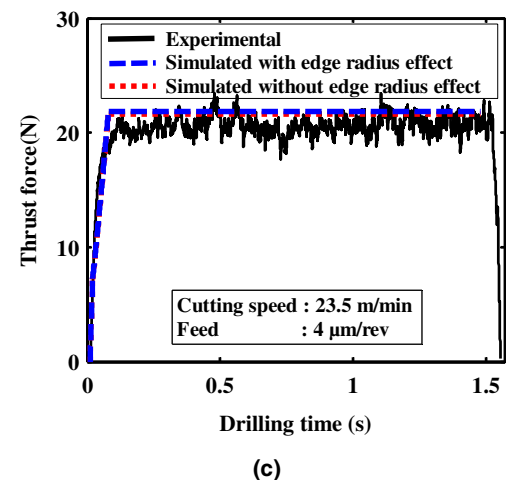
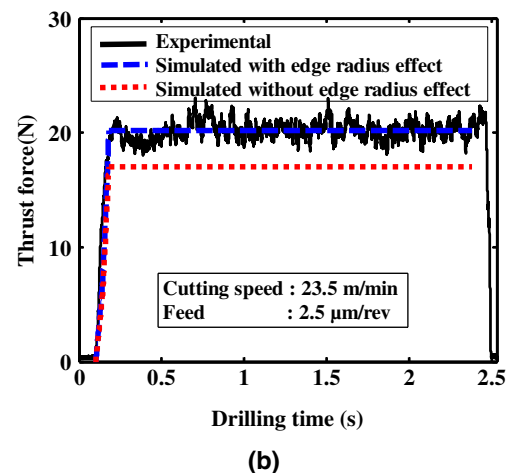
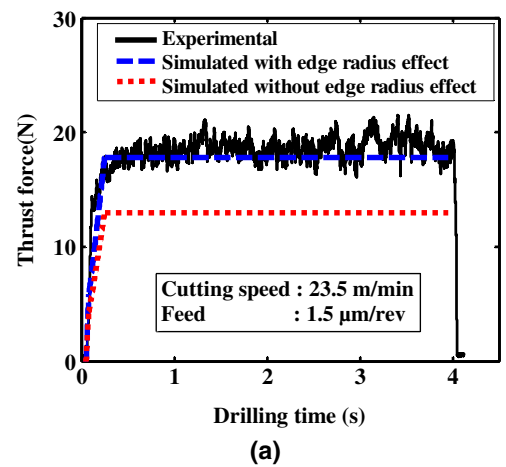
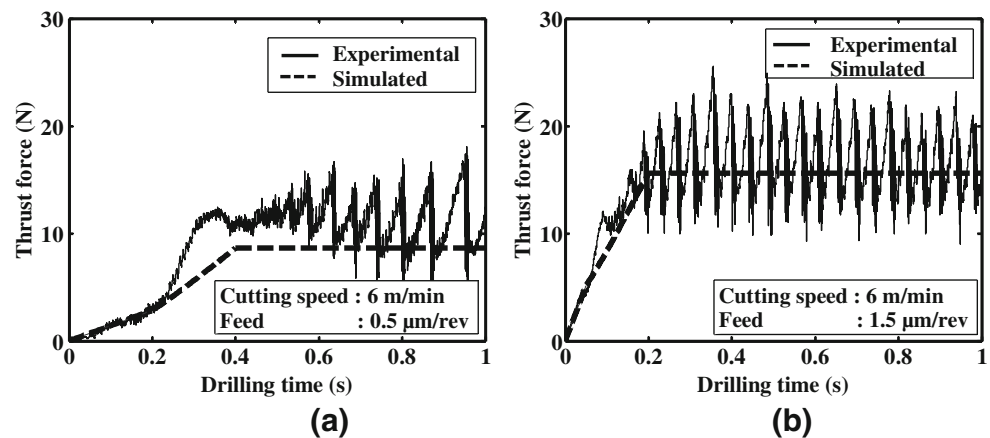


**Fig. 10** Comparison of prediction results in **a** ploughing region (feed 1.5  $\mu\text{m}/\text{rev}$ ), **b** transition region (feed 2.5  $\mu\text{m}/\text{rev}$ ), and **c** shearing region (feed 4  $\mu\text{m}/\text{rev}$ )

effective cooling and removal of chips from the cutting area. The proposed model with tool edge radius effects has been applied to simulate the thrust force signals obtained at cutting speed of 6 m/min and at low feed values of 0.5 and 1.5  $\mu\text{m}/\text{rev}$  as shown in Fig. 11a, b, respectively. The figures show that the

**Fig. 11** Experimental and simulated thrust force with feed **a** 0.5 and **b** 1.5  $\mu\text{m}/\text{rev}$  at 6 m/min cutting speed



model can predict the mean thrust at these two cutting conditions. The large fluctuations of the thrust force at these low feed cutting conditions may be due to the size effects. Chip removal does not take place in each rotation as uncut chip thickness values are less than minimum chip thickness. Thrust force is low as there is no chip removal and there is only ploughing/rubbing between the tool and workpiece. In the next rotation, accumulated chip thickness may be greater than the minimum chip thickness and chip removal takes place, and thus increase of thrust force can be observed. This cycle repeats till the end of the cutting process and helical chip is formed [29, 30]. However, this model takes care of only the mean value of the thrust force signals. The predicted mean thrust force values are in good agreement to the experimental mean thrust force values in all the cutting conditions tested here.

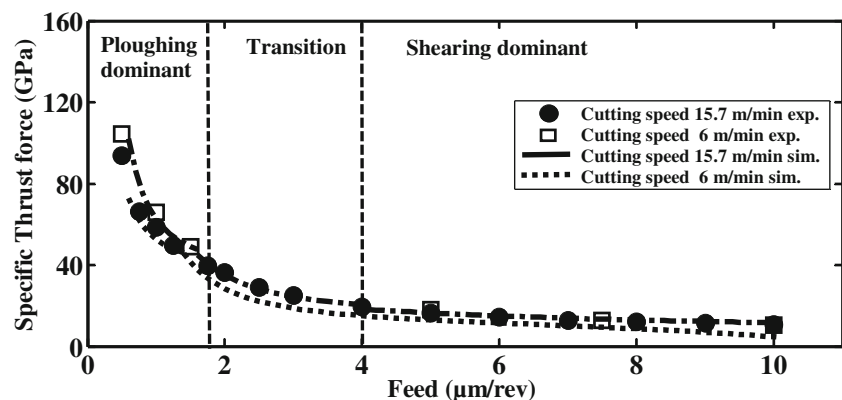
#### 4.2 Prediction of specific thrust force or size effects

In micro-machining, specific cutting force is generally measured to determine the size affect. Size effect in micro-machining earlier was characterized by nonlinear increase in specific cutting force for decreased undeformed chip thickness [5]. Specific cutting force in the feed direction as we call it “specific thrust force” is determined by dividing mean thrust

force by total chip area. The proposed mechanistic model has been applied to predict specific thrust force to characterize the size effects in micro-drilling of austenitic stainless steel. Figure 12 compares the experimental and predicted specific thrust forces for low to high feed values at two different cutting speeds (6 and 15.7 m/min). Even though these two cutting speeds have been selected from two different experimental setups of two different laboratories, the trends of specific thrust forces are same and their numerical values are also very close to each other. This obviously validates the reproducibility of the size effect phenomenon in micro-drilling process. Experimental and simulated specific thrust forces show good agreement to each other. The small deviation of the predicted specific thrust force values from the experimental results in case of 6 m/min cutting speed can be observed. This may be due the fact that selected cutting speed is outside the range of cutting speeds applied to calibrate the model constant. However, the trend of specific thrust force variation and its predicted values at low speed condition are within acceptable accuracy.

Figure 12 also shows how the specific cutting force increases nonlinearly when the undeformed chip thickness is equal or less than minimum chip thickness where the effective rake angle is highly negative and ploughing effect dominates in material removal process. Three cutting regions are

**Fig. 12** Variation of specific thrust force with feed at different cutting speed



separated based on the effective rake angle, and minimum chip thickness effect as explained earlier can also be observed from this figure. In the shear-dominant region, rate of change of specific cutting force is small as observed in the figure. On the other hand, the same increases in the transition region and becomes very high in ploughing-dominant region. The figure also shows that the model is able to capture the nonlinear behavior and increase in specific thrust forces near the transition and plowing-dominant regions.

## 5 Conclusion

A mechanistic micro-drilling force model has been developed with consideration of tool edge radius and minimum chip thickness effects. The model is applied to predict thrust force on a 500- $\mu\text{m}$  tungsten carbide drill for drilling of austenite stainless steel workpiece at various cutting conditions of two different machining environments. The mechanistic model has been calibrated and then validated by new experimental data. From this work, the following conclusions can be drawn:

1. The forces of micro-drilling can be modeled by the proposed mechanistic approach for the cases of both cutting with chip formation and ploughing without chip formation.
2. The proposed model has shown good conformity with experimental results for high uncut chip thickness to low uncut chip thickness even lower than the minimum chip thickness. The proposed model calibrated with data of one cutting environment has been shown to work well with prediction of cutting forces of micro-drilling experiments conducted in different cutting environment.
3. Specific cutting force has also been determined experimentally and predicted by the proposed mechanistic model. The results show that the proposed model can be applicable to characterize the size effects in micro-drilling process.
4. The proposed model has been limited to predict the mean thrust and mean specific force values as the drill dynamics has not been considered in this work. The future work should aim to develop dynamic model for micro-drilling considering the effects of drill vibration, drill run out, drill wandering, and various other factors.

**Acknowledgments** The authors would like to acknowledge the financial support offered by Department of Science & Technology (DST), Ministry of Science & Technology, Government of India, through SERC Fast Track Scheme (Project no. SR/FTP/ETA-0034/2010). The authors also acknowledge the financial support of the German Research Foundation (DFG) through a project grant on micro-machining of stainless steel (Project no. BI498/15-1) for the experiments carried out in Germany.

**Compliance with ethical standards** All professional ethics have been followed. The manuscript has not been submitted to other journal for simultaneous consideration. The manuscript has not been published previously (partly or in full). No data has been fabricated or manipulated and

no data, text, or theories by others are presented as if they were the author's own. Proper acknowledgements to other works have been given. Consent to submit has been received explicitly from all co-authors. Authors whose names appear on the submission have contributed sufficiently to the scientific work and therefore share collective responsibility and accountability for the results.

**Conflict of interest** There is no conflict of interest in this work.

**Human and animal rights and informed consent** This research does not involve any human or animal participant.

## References

1. Rahamathullah I, Shunmugam MS (2013) Analyses of forces and hole quality in micro-drilling of carbon fabric laminate composites. *J Comput Math* 47(9):1129–1140
2. Kuar AS, Acherjee B, Ganguly D, Mitra S (2012) Optimization of Nd:YAG laser parameters for microdrilling of alumina with multi quality characteristics via grey–taguchi method. *Mater Manuf Process* 27:329–336
3. Liow JL (2009) Mechanical micromachining: a sustainable micro-device manufacturing approach? *J Clean Prod* 17:662–667
4. Bissacco G, Hansen HN, Slunsky J (2008) Modelling the cutting edge radius size effect for force prediction in micro milling. *CIRP Ann Manuf Technol* 57:113–116
5. Aramcharoen A, Mativenga PT (2009) Size effect and tool geometry in micromilling of tool steel. *Precis Eng* 33:402–407
6. Vollertsen F, Biermann D, Hansen HN, Jawahir IS, Kuzman K (2009) Size effects in manufacturing of metallic components. *CIRP Ann Manuf Technol* 58:566–587
7. Chae J, Park SS, Freiheit T (2006) Investigation of micro-cutting operations. *Int J Mach Tools Manuf* 46:313–332
8. Klocke F, Gerschwiler K, Abouridouane M (2009) Size effects of micro drilling in steel. *Prod Eng Res Devel* 3:69–72
9. Anand RS, Patra K, Steiner M (2014) Size effects in micro drilling of carbon fiber reinforced plastic composite. *Prod Eng Res Devel* 8(3):301–307
10. Liu X, DeVor RE, Kapoor SG, Ehmann KF (2004) The mechanics of machining at the micro scale: assessment of the current state of the science. *J Manuf Sci Eng* 126:666–678
11. Anand RS, Patra K (2014) Modeling and simulation of mechanical micro-machining—a review. *Mach Sci Technol* 18:323–347
12. Rao S, Shunmugam MS (2012) Analytical modeling of micro end-milling forces with edge radius and material strengthening effects. *Mach Sci Technol* 16(2):205–227
13. Lai X, Li H, Li C, Lin Z, Jun N (2008) Modeling and analysis of micro scale milling considering size effect, micro cutter edge radius and minimum chip thickness. *Int J Mach Tools Manuf* 48:1–14
14. Jun MBG, Goo C, Malekian M, Park S (2012) A new mechanistic approach for micro end milling force modeling. *J Manuf Sci Eng* 134:1–97
15. Malekian M, Park SS, Jun MBG (2009) Modeling of dynamic micro-milling cutting forces. *Int J Mach Tools Manuf* 49:586–598
16. Hinds BK, Treanor GM (2000) Analysis of stresses in micro-drills using the finite element method. *Int J Mach Tools Manuf* 40:1443–1456
17. Gong Y, Lin C, Ehmann KF (2005) Dynamics of initial penetration in drilling: part 1—mechanistic model for dynamic forces. *J Manuf Sci Eng* 127:280–288

18. Sambhav K, Tandon P, Kapoor SG, Dhanda SG (2013) Mathematical modeling of cutting forces in microdrilling. *J Manuf Sci Eng* 135:014501
19. Kim DW, Lee YS, Park MS, Chu CN (2009) Tool life improvement by peck drilling and thrust force monitoring during deep-micro-hole drilling of steel. *Int J Mach Tools Manuf* 49:246–255
20. Zhang H, Wang X, Pang S (2014) A mathematical modeling to predict the cutting forces in microdrilling. *Math Probl Eng*, Article ID 543298, 11p
21. Rahamathullah I, Shunmugam MS (2014) Mechanistic approach for prediction of forces in micro-drilling of plain and glass-reinforced epoxy sheets. *Int J Adv Manuf Technol* 75:1177–1187
22. Flachs JR, Salahshoor M, Melkote SN (2014) Mechanistic models of thrust force and torque in step-drilling of Al7075-T651. *Prod Eng Res Devel* 8:319–333
23. Shaw MC (1992) *Metal cutting principles*, 1<sup>st</sup> Indian Edition, CBS Publ Distr. 428–486
24. Elhachimi M, Torbaty S, Joyot P (1999) Mechanical modelling of high speed drilling 1: predicting torque and thrust. *Int J Mach Tools Manuf* 39:553–568
25. Mauch CA, Lauderbaugh LK (1990) Modeling the drilling processes—an analytical model to predict thrust force and torque. *Proc Comput Model Simul Manuf Process* 48:59–65
26. Yuan ZJ, Zhou M, Dong S (1996) Effect of diamond tool sharpness on minimum cutting thickness and cutting surface integrity in ultraprecision machining. *J Mater Process Technol* 62:327–330
27. Liu X, DeVor RE, Kapoor SG (2006) An analytical model for the prediction of minimum chip thickness in micromachining. *J Manuf Sci Eng* 128:474–481
28. Patra K, Anand RS, Steiner M, Biermann D (2015) Experimental analysis of cutting forces in microdrilling of austenitic stainless steel (X5CrNi18-10). *Mater Manuf Process* 2: 248–255
29. Zheng L, Wang C, Yang L, Song Y, Fu L (2012) Characteristics of chip formation in the micro-drilling of multi-material sheets. *Int J Mach Tools Manuf* 52:40–49
30. Biermann D, Kirschner M, Eberhardt D (2014) A novel method for chip formation analyses in deep hole drilling with small diameters. *Prod Eng Res Devel* 8:491–497